Revealing fine structure in the antineutrino spectra from a nuclear reactor

A. A. Sonzogni, M. Nino, and E. A. McCutchan

Phys. Rev. C **98**, 014323 — Published 20 July 2018

DOI: 10.1103/PhysRevC.98.014323

Revealing Fine Structure in the Antineutrino Spectra from a Nuclear Reactor

A. A. Sonzogni,[1,*] M. Nino,[2] and E. A. McCutchan[1]

[1] *National Nuclear Data Center, Bldg. 817, Brookhaven National Laboratory, Upton, NY 11973-5000, USA*
[2] *Department of Physics and Astronomy, Hofstra University, Hempstead, NY 11549, USA*

(Dated: June 27, 2018)

We calculate the Inverse Beta Decay (IBD) antineutrino spectrum generated by nuclear reactors using the summation method to understand deviations from the smooth Huber-Mueller model due to the decay of individual fission products, showing that plotting the ratio of two adjacent spectra points can effectively reveal these deviations. We obtain that for binning energies of 0.1 MeV or lower, abrupt changes in the spectra due to the jagged nature of the individual antineutrino spectra could be observed for highly precise experiments. Surprisingly, our calculations also reveal a peak-like feature in the adjacent points ratio plot at 4.5 MeV even with a 0.25 MeV binning interval, which we find is present in the IBD spectrum published by Daya Bay in 2016. We show that this 4.5 MeV feature is caused by the contributions of just four fission products, ^{95}Y, ^{98,101}Nb and ^{102}Tc. This would be the first evidence of the decay of a few fission products in the IBD antineutrino spectrum from a nuclear reactor. This result is supported by applying the same numerical technique to the measured aggregate electron spectra.

I. INTRODUCTION

Since the discovery of radioactivity in 1895 [1], scientists have been able to accurately characterize the γ, e^-, e^+, neutron, proton and α spectra emitted by nuclei during their radioactive decay. However, measuring the antineutrino spectra from the decay of individual nuclei has eluded experimental efforts even today as antineutrinos only interact with matter through the weak interaction. The closest direct measurements of neutrino spectra following beta-decay are the neutrino oscillation measurements of the SNO experiment [2] which measured neutrinos following solar ^{8}B decay. However, the energy distribution of antineutrinos from a single nucleus following β-minus decay has not been reported to the best of our knowledge. There has been, nevertheless, tremendous success in detecting antineutrinos from nuclear reactors starting with the pioneering work of Cowan and Reines [3]. Most recently, the Daya Bay [4], Double Chooz [5], and RENO [6] collaborations have measured reactor's antineutrino spectra with unprecedented statistics by placing large detectors near commercial reactors. In these experiments, antineutrinos are produced by the approximately 800 fission products, and are later detected using the Inverse Beta Decay (IBD) reaction, $\overline{\nu}_e + p \rightarrow n + e^+$. Since the IBD cross section increases steadily for energies above its 1.8 MeV threshold, and as the antineutrino spectrum generated by a reactor decreases with increasing energy, the resulting IBD spectrum has a bell shape with the maximum around 3.5-4.0 MeV.

The focus in the interpretation and understanding of these reactor experiments has been through comparing the integral and overall shape of the measured spectrum to various predictions. Currently, the antineutrino spectra from Huber [7] for ^{235}U, ^{239,241}Pu, obtained from converting measured aggregate electron spectra [8–10], and from Mueller *et al.* [11] for ^{238}U derived from nuclear databases, are considered the best predictions. Comparisons of measured IBD spectra with the Huber-Mueller model have revealed an overall deficit in the number of measured antineutrinos along with a spectra distortion [12]. These findings then spurred a flurry of investigations into the source of these disagreements [13–19].

A new generation of experiments at very short baselines [21, 22, 41] have begun or will soon begin to collect data near a reactor core to study the possible existence of sterile neutrinos, as well as to gauge antineutrinos' potential to monitor nuclear reactors [23, 24]; moreover, the potential of antineutrino detectors to aid in the identification of nuclear explosions has also been discussed [25]. Of particular interest for this work are the recently published results from the NEOS collaboration [22], which reported an IBD spectrum with a binning interval of 0.1 MeV, that is, a considerable improvement over the 0.20 - 0.25 MeV values that have been the standard so far.

In this work we will not address the overall deficit of antineutrinos nor the excess observed in the 5-7 MeV region. Instead, motivated by the presence of sharp deviations in the NEOS IBD spectrum from the smooth Huber-Mueller predictions near the maximum, we explore the possibility of observing signatures of the individual fission products amidst the overall spectrum, which in vague analogy with other radiation types, we will refer to as "fine structure". In an attempt to view the trees from the forest, we present a novel approach to analyzing antineutrino spectra which involves taking ratios of adjacent energy bins. We then apply this technique to the highest resolution data available from the Daya Bay collaboration and find that even with a 0.25 MeV binning, fine structure in the antineutrino spectra is evident and moreover, is in agreement with calculations which consider the decay of all fission fragments produced in the reactor. This fine structure can be attributed to just a few nuclei, suggesting that

* sonzogni@bnl.gov

indeed the individual signatures of the fission fragments can be unraveled from the whole. Applying the same numerical technique, we also find evidence of fine structure in the aggregate electron spectra.

II. FORMALISM

Electrons and antineutrinos are produced in a nuclear reactor following the β^- decay of neutron rich fission products, whose sum spectra can be calculated using the summation method [26] as

$$S(E) = \sum_i \sum_j f_i \times CFY_{ij} \times S_j(E), \quad (1)$$

where f_i are the effective fission fractions for the four main fuel components, ^{235}U, ^{238}U, ^{239}Pu and ^{241}Pu; CFY_{ij} are the cumulative fission yields from the neutron induced fission on these fissile nuclides; and the spectra $S_j(E)$ are calculated as

$$S_j(E) = \sum I_{jk} \times S_{jk}(E), \quad (2)$$

with I_{jk} the β^- decay intensity from the jth β^- decaying level in the network to the kth level in the daughter nucleus, and $S_{jk}(E)$ are the corresponding nuclear level to nuclear level spectra, which for electrons are given by

$$S(E) = N \times W \times (W^2-1)^{1/2} \times (W-W_0)^2 \times F(Z,W) \times C(Z,W), \quad (3)$$

where N is a constant so that $S(E)$ is normalized to unity; W is the relativistic kinetic energy, $W = E/m_ec^2+1$, and W_0=Q/m_ec^2+1, with Q the total decay energy available also known as the end-point energy; $F(Z,W)$ is the Fermi function and Z is the number of protons in the daughter nucleus; lastly, the $C(Z,W)$ term contains the corrections due to angular momentum and parity changes, finite size, screening, radiative and weak magnetism.

The $W \times (W^2-1)^{1/2} \times (W-W_0)^2$ product in Eq. (3) is colloquially known as the "phase space" term as it is customarily inferred using statistical classical mechanics arguments. In the absence of Coulomb effects, the electron and antineutrino spectra would be given by this term, resulting in identical energy distributions, as seen in Fig. 1 (a). The proton's Coulomb field gives rise to the Fermi function term, F(Z,W), which slows down the electrons. Conservation of energy then dictates a corresponding boost to the antineutrino energy. The effect for electrons can be seen in Fig. 1 (b), while Fig. 1 (c) shows the antineutrino spectra. Because of the Fermi function, the level-to-level antineutrino spectra exhibit an abrupt cutoff at the end-point energy. As a consequence, while a sum of electron spectra will have a smooth quality, a sum of antineutrino spectra may have a rugged, serrated nature. Fig. 1 also reveals that the cut-off in the antineutrino spectrum is more severe for lower-energy antineutrinos, being particularly pronounced for end point

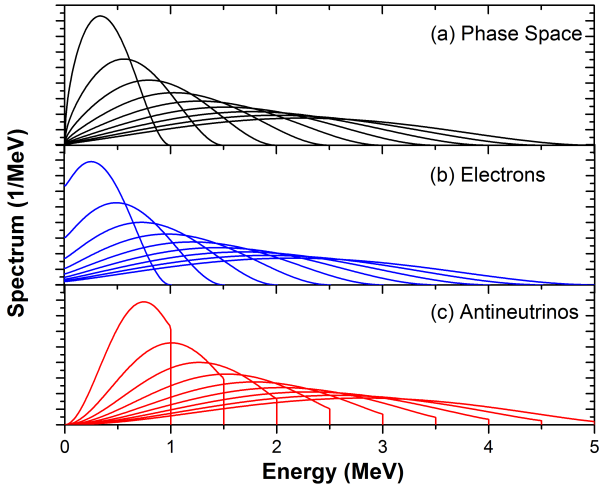

FIG. 1. (a) Energy distribution using only the phase space term, (b) energy distribution for electrons including all the correction terms (c) as the middle panel but for antineutrinos.

energies between 1 and 3 MeV, and with increasing end point energy the serrated portion of the spectrum quickly diminishes.

III. RESULTS

Producing a neutron-rich source of a single isotope, strong enough to observe the intriguing features in Fig. 1 (c), would be experimentally extremely challenging. The question is, within the 800 fission fragments (with 10 to 100's of β branches) produced in a nuclear reactor, can the spectra from individual nuclei be disentangled. We explore this possibility by calculating the antineutrino spectra for the Daya Bay experiment with the summation method using: (a) Daya Bay fission fractions [4]; (b) JEFF-3.1 fission yields [27] and updated ENDF/B-VII.1 decay data [28] as described in Refs. [29, 30]; (c) $F(Z,W)$ and $C(Z,W)$ as given by Huber [7]; (d) IBD cross sections from Ref. [31]. The resulting IBD antineutrino spectrum is shown in Fig. 2 (a), plotted together for contrast with the corresponding Huber-Mueller spectrum (shifted down). The energy range was restricted to 2.5 to 5.5 MeV, where statistical uncertainties will be sufficiently low to allow the observation of fine structure.

Hints of fine structure begin to materialize in the summation calculation around 2.8 MeV; the most obvious is a sharp cutoff just below 3.5 MeV, which corresponds to the sharp cutoffs seen in Fig. 1(c). There is also another type of structure that spans several hundreds of keV, such as a shoulder around 4.2 to 4.5 MeV, which would correspond to the contribution of a single fission product or a group of them that have similar end point energies. The role of binning in our summation calculations, not

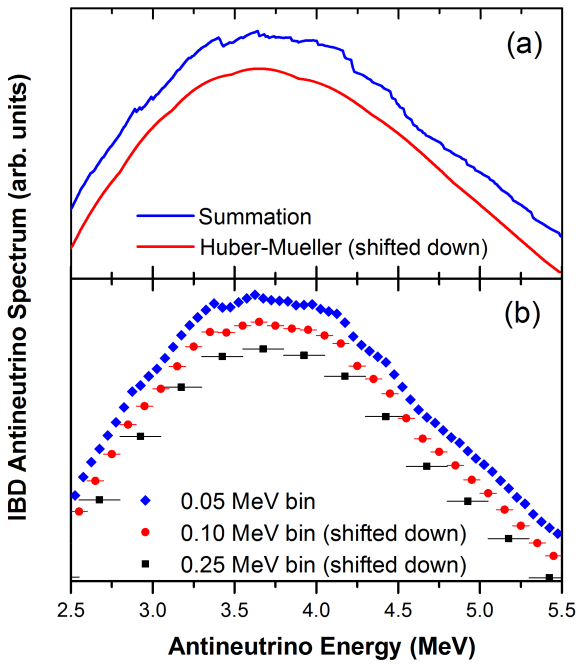

FIG. 2. (a) Calculated Daya Bay IBD antineutrino spectra using the summation method (top blue line) and the Huber-Mueller antineutrino spectra (lower red line), shifted down to highlight the jaggedness of the former versus the smoothness of the latter. (b) IBD antineutrino spectra from summation calculations binned in 0.05, 0.10 and 0.25 MeV intervals. For contrast reasons, the last two datasets are shifted down. Note that this figure is a truncated plot of the full IBD spectrum highlighting the 2.5 to 5.5 MeV energy range.

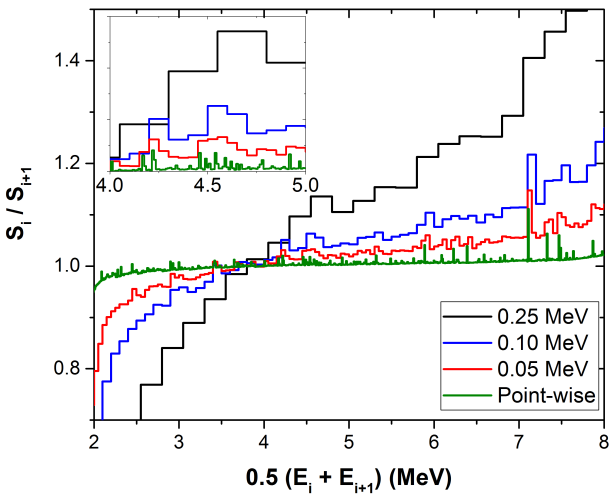

FIG. 3. Ratio of two consecutive summation IBD spectrum points under different binning conditions. A zoom in the 4 to 5 MeV region can be seen in the top-left corner inset.

including experimental resolution nor counting statistics effects, is explored in Fig. 2 (b), where with 0.25 MeV binning intervals, used by Daya Bay, deviations from a smooth curve would be hard to discern by eyesight, while with 0.10 MeV bins, as available in NEOS [22], fine structure would manifest and become clearer with a 0.05 keV binning. A similar analysis as a function of the detector resolution was presented in Ref. [32].

While there are definite features in the spectra shown in Fig. 2, they are difficult to interpret quantitatively. To better elucidate fine structure, we have explored different numerical approaches, and concluded that the a satisfactory elucidation can be obtained using the ratio of adjacent points

$$R_i = S_i/S_{i+1}, \tag{4}$$

as a function of the average bin interval $0.5\times(E_i+E_{i+1})$. These values are plotted in Fig. 3 for a summation IBD spectrum, under different binning scenarios. For a point-wise calculation, the sudden drop in the spectrum due to the abrupt end of a relevant fission product antineutrino spectrum would manifest as a peak, for instance that of ^{96}Y at 7.1 MeV, whose signature can also be seen with 0.05 and 0.1 MeV binning. Intuitively, it may be thought that for a 0.25 MeV binning, a smooth curve would be obtained. However, a peak-like feature around 4.5 MeV is visible, which as the inset in the top-left corner reveals, it is caused by a number of strong transitions that coincidentally have similar end-point energies. Inspired by this observation, the Daya Bay R_i values are plotted in Fig. 4, with uncertainties calculated as

$$\begin{aligned}\Delta^2 R_i =& S_{i+1}^{-2}\times\sigma_{i,i} + S_i^2\times S_{i+1}^{-4}\times\sigma_{i+1,i+1} \\ &- 2\times S_i\times S_{i+1}^{-3}\times\sigma_{i,i+1},\end{aligned} \tag{5}$$

with σ the covariance matrix as given by the Daya Bay Collaboration [4]. The need of the covariance matrix is significant here since as the adjacent S_i points are positively correlated, that is $\sigma_{i+1,i+1} > 0$, the ΔR_i values are smaller than those obtained assuming no correlation, which definitely helps in the positive identification of the structures in the R_i plot. We note that 4.5 MeV peak-like feature in the summation calculation remains unchanged if an energy resolution of $0.07\%\times(E_{prompt})^{1/2}$ and counting statistics of 3×10^5 events are included in a simulation.

While the summation χ^2/point in Fig. 4 is only marginally smaller than Huber-Mueller's, 2.0 vs. 2.4 for the whole energy range and 4.2 vs. 6.3 in the in the 4.1 to 5.6 MeV region, the summation calculation shape is remarkably more similar to the experimental one. This demonstrates the necessity to improve the summation method, which despite being less precise than the conversion method due to deficiencies in fission yield and decay data [33], is absolutely needed to fully understand the features of a reactor antineutrino spectrum.

The next question is if can we attribute the 4.5 MeV peak-like feature to individual nuclei. To answer this, we searched for the most relevant individual IBD spectra with large R values around 4-5 MeV. We find that the feature at 4.5 MeV is caused by just four nuclides, ^{95}Y,

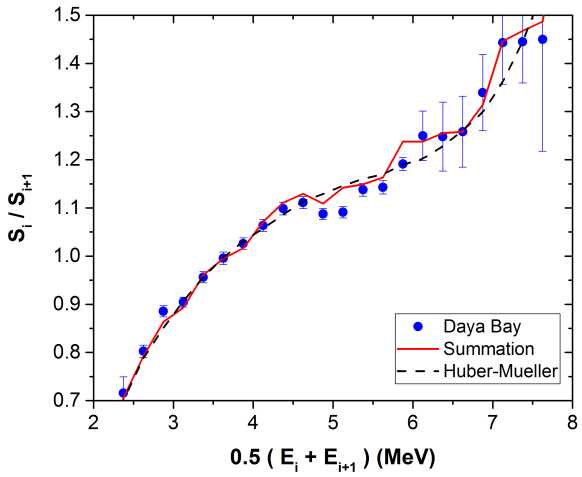

FIG. 4. Ratio of two consecutive IBD spectrum points from the Daya Bay experiment (symbols), Huber-Mueller model (dashed black line) and summation method (full red line). For clarity's sake, the calculated points are connected with a straight line, instead of a step function as in Fig. 3.

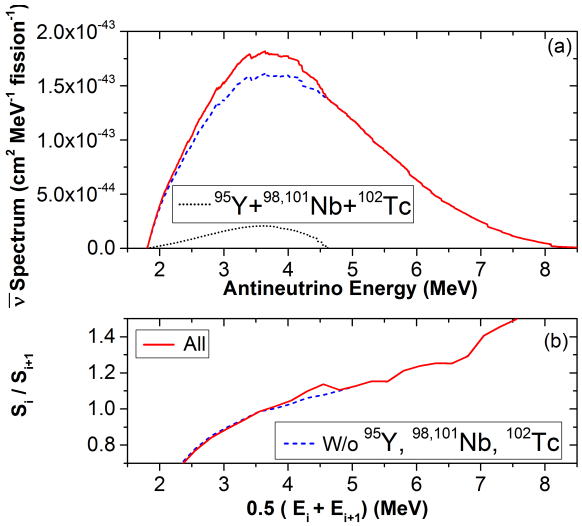

FIG. 5. (a) Calculated Daya Bay IBD antineutrino spectra from all the fission products (full red line), the ^{95}Y, ^{98,101}Nb, and ^{102}Tc contribution (dotted black line), and the difference (dashed blue line). (b) Corresponding ratio of two adjacent points with a 0.25 MeV binning.

^{98,101}Nb, and ^{102}Tc, having in common large cumulative fission yields and antineutrino spectra dominated by strong transitions with end-point energies near 4.5 MeV. The reason why only four nuclides are responsible for this effect is mainly due to the double-humped nature of the independent fission yield distributions, resulting in a relatively small number of nuclides with significant effective cumulative fission yields, $CFY_{eff,i} = \sum f_k CFY_{ki}$. For instance, for the Daya Bay fission fractions, the largest effective CFY for products contributing to the IBD spectrum is that of ^{134}I with $CFY_{eff,i}$=0.073. While the number of nuclides with effective CFYs larger than 0.01 is about 115, it drops to about 30 for effective CFYs larger than 0.05. This number is further reduced when we require these nuclides to have large values of I_{ki} with end-point energies in the 4 to 5 MeV region. Fig. 5 (a) shows the total IBD spectrum, the one generated by the four nuclides in question, and the difference. These four nuclides account for about 6% of the total IBD antineutrino yield, and about 9.6% of the IBD antineutrino yield in the 1.8 to 4.5 MeV region. Fig. 5 (b) shows a plot of R_i values with a 0.25 MeV binning with and without the contribution of ^{95}Y, ^{98,101}Nb, and ^{102}Tc, which clearly shows that the feature at 4.5 MeV is basically caused by these four nuclides.

As prior works have investigated the need for reliable decay and fission yield data [29, 33, 34] to accurately calculate antineutrino spectra, we now assess the quality of the ^{95}Y, ^{98,101}Nb, and ^{102}Tc data to determine if the 4.5 MeV structure in the summation calculations is a solid prediction. The effective JEFF CFYs for these nuclides, with relative uncertainty in parenthesis, are 0.058 (0.9%), 0.057 (3.4%), 0.054 (1.9%), and 0.050 (3.7%) respectively. The ENDF/B-VII.1 effective cumulative fission yields are similar, within 2% from the JEFF values, with the exception of ^{102}Tc, whose independent fission yield is considerably smaller than its cumulative as it is mainly produced in the decay of ^{102}Mo. When the ENDF/B yields were obtained, it was assumed that the isomer would take most of the β-decay intensity, which as we know today it is not the case. When this correction is applied, both values of cumulative fission yields agree very well. In terms of the decay data for these four nuclides, the β intensity pattern is dominated by a strong ground state (GS) to ground state transition with end point energies near 4.5 MeV. In more detail, GS to GS transitions intensities and Q-values are: 64±1.7% and 4.45 MeV for ^{95}Y [35], 57±7% and 4.59 MeV for ^{98}Nb [36], 40±13% and 4.55 MeV for ^{101}Nb [37], 92.9±0.6% and 4.53 MeV for ^{102}Tc [38, 39]. We conclude that the nuclear data for these four nuclides are fairly reliable due to the relative closeness to the valley of stability.

Further insights can be obtained by studying Fig. 6, where the IBD antineutrino spectra for all fission products are plotted, highlighting the ^{95}Y, ^{98,101}Nb and ^{102}Tc spectra. Due to the similar end-point energies, their sum spectrum effectively looks like that of a single strongly produced fission product. For comparison, the three largest spectra are labeled, which contribute 6.7% (^{92}Rb), 5.3% (^{96}Y) and 4.1% (^{100}Nb) to the total IBD antineutrino yield. Despite their sizable contribution, observing the fine structure from their antineutrino spectra sharp cutoff would be considerably more difficult as the relative importance of the sharp cutoff diminishes and the IBD antineutrino spectrum is considerably smaller at energies close to their end-point energies.

These trees hiding in the forest of all the fission fragments should in principle also be present in the precise

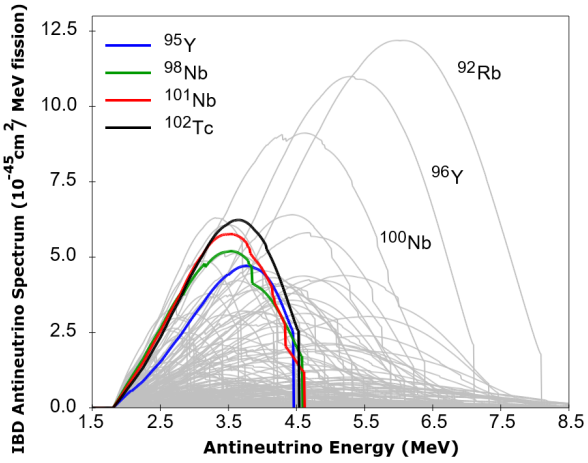

FIG. 6. Calculated IBD antineutrino spectra from all the fission products, highlighting the ^{95}Y, ^{98,101}Nb, and ^{102}Tc ones.

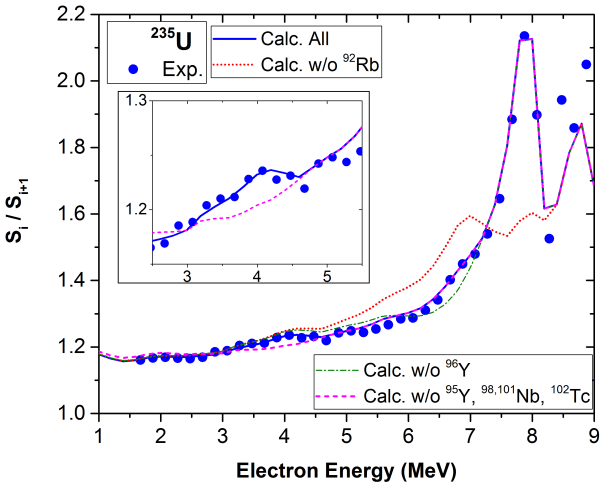

FIG. 7. Ratio of adjacent ^{235}U electron spectrum points binned with a 200 keV interval using experimental data from Ref. [9]. The solid blue line corresponds to a summation calculation including all fission products, while the remaining lines correspond to summation calculations where the contribution from one or more fission products has been subtracted. The inset shows the 2.5 to 5.5 MeV region to highlight the ^{95}Y, ^{98,101}Nb and ^{102}Tc effect on the summation calculations.

measurements of the electron spectra performed at the Institute Laue-Langevin [8–10], which constitute the foundation of the antineutrino spectra derived by Huber using the conversion method. Armed with the experience obtained finding fine structure in the Daya Bay antineutrino spectrum, we will focus out attention on ^{235}U, whose electron spectrum has been measured with a finer step and smaller uncertainty than those of ^{239}Pu and ^{241}Pu; our conclusions, however, are also valid for the Pu nuclides. We plot in Fig. 7 the ratio of adjacent ^{235}U electron spectra with 200-keV binning together with summation calculations including all fission products as well as excluding a few relevant cases which helps reveal heretofore unrecognized features. For simplicity's sake, and also because of the lack of the spectrum's correlation matrix, uncertainties are not shown. The inset to Fig. 7 shows the energy region expanded around 4 MeV. A peak is again present around 4 MeV (recall that a shift of about 0.5 MeV between electron and antineutrino spectra arises from Coulomb effects) which is well described by the summation calculation including ^{95}Y, ^{98,101}Nb and ^{102}Tc. When these nuclei are excluded from the calculation, the summation calculation becomes featureless. A peak-like structure is also clearly seen at around 8 MeV. A comparison between the full summation calculation with the one that excludes ^{92}Rb (blue vs red curves), clearly shows that the peak at around 7.8 MeV originates from this nucleus. Additionally, the shoulder at around 7 MeV is produced by ^{96}Y (blue vs green curves). This analysis, complementary to the one presented earlier for the antineutrino spectra, clearly shows that with the proper numerical method, comprehensive nuclear databases, and highly precise data, seemingly featureless spectra can reveal plenty of details.

Finally, we discuss another fine structure effect that can surface when combining the 2016 Daya Bay data with a smaller binning data, as was done by the NEOS collaboration when performing a 3+1 ν model parameter fit [22]. Unfortunately, this data is unavailable in numerical form and presented as a function of prompt energy only. Analysis of this data has therefore relied on ratios to either the Huber-Muller model or the Daya Bay prompt energy spectrum [40]. To start, we calculate the summation antineutrino spectra for the Daya Bay and NEOS fission fractions with 100 keV and 250 MeV binning intervals without including resolution and counting statistics effects; then we calculate the Daya Bay spectrum corresponding to the NEOS fission fractions using a first order Taylor expansion on the fission fractions [4]

$$S_{DBC} = S_{DB} + \sum S_i^{HM} \times (f_i^{NEOS} - f_i^{DB}), \quad (6)$$

where S_i^{HM} are the Huber-Mueller antineutrino spectra for the 4 fissile nuclides. We then obtain the antineutrino spectra ratio between different 100 keV and the 250 keV binning combinations, using a linear interpolation in the latter, as can be seen in Fig. 8. Several observations can be made (a) the NEOS/DB curve is above 1 as NEOS has a larger ^{235}U fission fraction, (b) the peak at 2 MeV has no physical meaning, arising spuriously from the numerical methods used, (c) the lack of smoothness in the NEOS/DB and NEOS/DBC curves for energies above 2.5 MeV are due to fine structure. As a consequence, the peak-like features observed at 2.5 MeV and 3.25 MeV in the lower panel of Fig. 3 in Ref. [22] may not be included in 3+1 ν fit as they may be caused by contributions of individual fission products revealed in a finer binning.

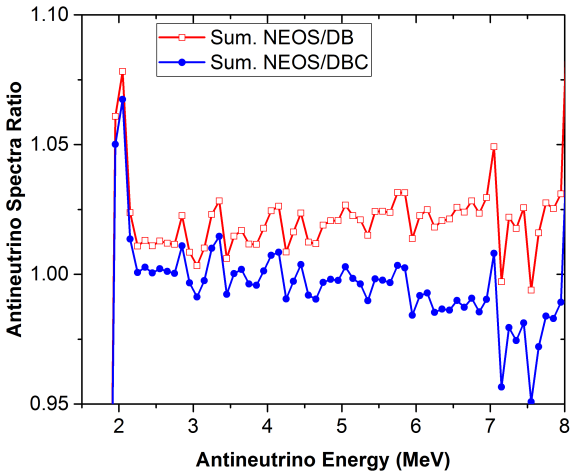

FIG. 8. Ratio of 100-keV to 250-keV binned summation antineutrino spectra. The red, open symbol curve corresponds to the ratio of the NEOS to the Daya Bay data, while the blue, full symbol curve corresponds to the the ratio of the NEOS to the fission fraction corrected Daya Bay data.

IV. CONCLUSIONS

In summary, we have shown that deviations in the IBD antineutrino spectrum from a nuclear reactor from a smooth shape can arise due to (a) the contribution of a strongly populated fission product, (b) sharp cutoffs in the individual antineutrino spectra, and (c) the contribution from a small number of fission products with similar end-point energy, effectively mimicking the first case. We developed a novel, yet simple way of numerically revealing these contributions, by plotting the ratio of adjacent points. We conclude that with a binning interval of 0.1 MeV or less, the observation of sharp cutoffs from the individual spectra could be attained. Remarkably, even with a binning of 0.25 MeV, we are able to detect a peak-like feature in the ratio plot, which we can attribute to the decay of ^{95}Y, ^{98,101}Nb and ^{102}Tc. Applying the same technique on the aggregate electron spectra confirms our observations. Finally, we have also shown that with the appropiate resolution, fine structure effects could be present in the ratio of a 100-keV binned IBD antineutrino spectrum to the 2016 Daya Bay one simply due to a reduction in the binning interval.

Soon, the next generation of antineutrino detectors, like PROSPECT [41], will provide high-statistics antineutrino spectra where the type of features discussed in the present article should be even more prevalent. This article clearly shows the need for highly reliable fission and decay data to fully understand all the features in the IBD antineutrino spectrum from a nuclear reactor as the smooth parameterization in the Huber-Mueller spectra can not account for individual nuclide effects. In addition, higher statistics data in the 6 to 8.5 MeV range should allow the effect of ^{96}Y and ^{92}Rb to be revealed and potentially shed light on the spectral anomaly.

ACKNOWLEDGMENTS

Work at Brookhaven National Laboratory was sponsored by the Office of Nuclear Physics, Office of Science of the U.S. Department of Energy under Contract No. DE-AC02-98CH10886, and by the DOE Office of Science, Office of Workforce Development for Teachers and Scientists (WDTS), under the Science Undergraduate Laboratory Internships Program (SULI). This work was partially supported under the U.S. Department of Energy FIRE Topical Collaboration in Nuclear Theory.

We are grateful to the Daya Bay collaboration for publishing their measured IBD antineutrino spectrum with corresponding covariance matrix as function of the antineutrino energy, which have made possible the analysis presented in this article.

[1] M. H. Becquerel, C. R. Physique **122**, 420 (1896).
[2] Q. R. Ahmad *et al.*, Phys. Rev. Lett. **87**, 071301 (2001).
[3] C. L. Cowan, Jr., F. Reines, F. B. Harrison, H. W. Kruse, A. D. McGuire, Science, **24**, Number 3212, 103 (1956).
[4] F. P. An *et al.*, Phys. Rev. Lett. **116**, 061801 (2016).
[5] Y. Abe *et al.*, Phys. Rev. Lett. **108**, 131801 (2012).
[6] J. H. Choi *et al.*, Phys. Rev. Lett. **116**, 211801 (2016).
[7] P. Huber, Phys. Rev. C **84** 024617 (2011).
[8] F. von Feilitzsch, A. A. Hahn, and K. Schreckenbach, Phys. Lett. B **118**, 162 (1982).
[9] K. Schreckenbach *et al.*, Phys. Lett. B **160**, 325 (1985).
[10] A. A. Hahn *et al.,* Phys. Lett. B **218**, 365 (1989).
[11] T. A. Mueller *et al.,* Phys. Rev. C **83**, 054615 (2011).
[12] G. Mention *et al.,* Phys. Rev. D **83**, 073006 (2011).
[13] A. C. Hayes *et al.,* Phys. Rev. Lett. **112**, 202501 (2014).
[14] A. C. Hayes *et al.,* Phys. Rev. D **92**, 033015 (2015).
[15] P. Huber, Phys. Rev. Lett. **118**, 042502 (2017).
[16] F. P. An *et al.*, Phys. Rev. Let. **118**, 251801 (2017).
[17] A. A. Sonzogni, E. A. McCutchan, and A. C. Hayes, Phys. Rev. Lett. **119**, 112501 (2017).
[18] G. Mention, M. Vivier, J. Gaffiot, T. Laserre, A. Letourneau, T. Materna, Phys. Lett. B **773**, 307 (2017).
[19] A. C. Hayes, G. Jungman, E. A. McCutchan, A. A Sonzogni, G. T. Garvey, and X. B. Wang, Phys. Rev. Lett. **120**, 022503 (2018).
[20] J. Ashenfelter *et al.,* Nucl. Instrum. Methods Phys. Res., Sect. A **806**, 401 (2016).
[21] G. Boireau *et al.*, Phys. Rev. **D** 93, 112006 (2016).
[22] Y. Ko *et al.*, Phys. Rev. Lett. **118**, 121802 (2017).
[23] E. Christensen, P. Huber, P. Jaffke, and T.E. Shea, Phys. Rev. Lett. **113**, 042503 (2014).
[24] M. Askins, *et al.*, arXiv:1502.01132 (2015).
[25] R. Carr, F. Dalnoki-Veress, and A. Bernstein, ArXiv 1712.04001 (2017).

[26] P. Vogel *et al.*, Phys. Rev. C **24**, 1543 (1981).
[27] M. A. Kellett, O. Bersillon, and R.W. Mills, JEFF REPORT 20, OECD, ISBN 978-92-64-99087-6 (2009).
[28] M. B. Chadwick *et al.*, Nucl. Data Sheets **112**, 2887 (2011).
[29] A. A. Sonzogni, T. D. Johnson, and E. A. McCutchan, Phys. Rev. C **91**, 011301(R) (2015).
[30] A. A. Sonzogni, E. A. McCutchan, T. D. Johnson, and P. Dimitriou, Phys. Rev. Lett. **116**, 132502 (2016).
[31] A. Strumia and F. Vissani, Phys. Lett. B **564**, 42 (2003).
[32] D. A. Dwyer and T. J. Langford, Phys. Rev. Lett **114**, 012502 (2015).
[33] M. Fallot *et al.*, Phys. Rev. Lett. **109**, 202504 (2012).
[34] B. C. Rasco *et al.*, Phys. Rev. Lett. **117**, 092501 (2016).
[35] S. K. Basu, G. Mukherjee, and A. A. Sonzogni, Nucl. Data Sheets **111**, 2555 (2010).
[36] B. Singh, and Z. Hu, Nucl. Data Sheets **98**, 335 (2003).
[37] J. Blachot, ENSDF database, www.nndc.bnl.gov/ensdf.
[38] D. De Frene, Nucl. Data Sheets **110**, 1745 (2009).
[39] D. Jordan *et al.*, Phys.Rev. C **87**, 044318 (2013).
[40] P. Huber, Phys. Rev. Lett. **118**, 042502 (2017).
[41] J. Ashenfelter *et al.*, J. Phys. G: Nucl. Part. Phys. **43**, 113001 (2016).